Journal of Molecular Structure 972 (2010) 41–50

Contents lists available at ScienceDirect

Journal of Molecular Structure

journal homepage: www.elsevier.com/locate/molstruc

Shape-dependent global deformation modes of large protein structures

Gennady V. Miloshevsky [a,*], Ahmed Hassanein [a], Peter C. Jordan [b,*]

[a] School of Nuclear Engineering, Purdue University, West Lafayette, IN 47907, USA
[b] Department of Chemistry, MS-015 Brandeis University, P.O. Box 549110, Waltham, MA 02454-9110, USA

ARTICLE INFO

Article history:
Received 23 November 2009
Received in revised form 3 January 2010
Accepted 5 January 2010
Available online 11 January 2010

Keywords:
Minimization
Normal modes
Conformational changes
Gating transitions
Protein shape
Mode following

ABSTRACT

Conformational changes are central to the functioning of pore-forming proteins that open and close their molecular gates in response to external stimuli such as pH, ionic strength, membrane voltage or ligand binding. Normal mode analysis (NMA) is used to identify and characterize the slowest motions in the gA, KcsA, ClC-ec1, LacY and $LeuT_{Aa}$ proteins at the onset of gating. Global deformation modes of the essentially cylindrical gA, KcsA, LacY and $LeuT_{Aa}$ biomolecules are reminiscent of global twisting, transverse and longitudinal motions in a homogeneous elastic rod. The ClC-ec1 protein executes a splaying motion in the plane perpendicular to the lipid bilayer. These global collective deformations are determined by protein shape. New methods, all-atom Monte Carlo Normal Mode Following and its simplification using a rotation–translation of protein blocks (RTB), are described and applied to gain insight into the nature of gating transitions in gA and KcsA. These studies demonstrate the severe limitations of standard NMA in characterizing the structural rearrangements associated with gating transitions. Comparison of all-atom and RTB transition pathways in gA clearly illustrates the impact of the rigid protein block approximation and the need to include all degrees of freedom and their relaxation in computational studies of protein gating. The effects of atomic level structure, pH, hydrogen bonding and charged residues on the large-scale conformational changes associated with gating transitions are discussed.

1. Introduction

X-ray crystallography [1] yields atomically resolved protein structures in near-native conformations; these can be explored to illuminate protein structure–function relationships. Although such structures, captured in a variety of conformations, provide useful architectural insights, they remain only static images of dynamic systems. To understand protein function requires characterizing dynamic behavior during conformational changes (gating) that permit signaling (ion channels) or substrate transport (transporters). Experimentally derived B-factors [2,3] identify highly mobile regions, but these are often flexible polypeptide loops and protein blocks not necessarily involved in gating. In addition, B-factors are not vectorial, and cannot provide insight into gating movements. Fluorescent resonance energy transfer and nuclear magnetic resonance methods [4,5] can provide partial information with respect to the directionality of conformational changes, but full dynamical detail is unresolved. Molecular modeling approaches such as molecular dynamics (MD) simulations [6] and normal mode analysis (NMA) [7] are also used to study protein conformational dynamics.

Reliable computational sampling of gating transitions is a long-standing challenge [8]. There are two distinct difficulties. First, transitions are many orders of magnitude slower than atomic vibrations. Second, nature tends to be perverse, and crystallography usually provides conformational data for only one of many functionally important states. Thus, not only is standard MD, limited to nsec simulations, an inadequate analytical tool but it is also generally necessary to "bootstrap" migration on a potential energy surface for which the reliable experimental data only characterizes a single functionally important configuration. Numerous approaches have been devised to address these issues. If two conformational endpoints are known, a new technique [9,10], carrying out repeated trajectory analysis at successive points along a transition pathway is a promising MD extension of line search methods [7] for migrating on complex potential surfaces. However, the more typical situation is a single endpoint structure established crystallographically. In steered MD, a probable direction for gating is arbitrarily designated; however, the imposed high-speed perturbations have recently been shown to introduce intrinsic bias in the simulations [11]. All-atom NMA [12,13], coarse-grained Gaussian Elastic Network models [13,14] and Principal Component Analysis [15,16] are useful techniques for identifying large-scale protein motions. However, they only identify the initial steps in exiting a

* Corresponding authors. Tel.: +1 765 494 8618; fax: +1 765 496 2233 (G.V. Miloshevsky); tel.: +1 781 736 2540; fax: +1 781 736 2516 (P.C. Jordan).
E-mail addresses: gennady@purdue.edu (G.V. Miloshevsky), jordan@brandeis.edu (P.C. Jordan).

0022-2860/$ - see front matter © 2010 Elsevier B.V. All rights reserved.
doi:10.1016/j.molstruc.2010.01.009

near-native protein conformation, and thus only probe the onset of a gating transition. In these applications a target structure is usually generated from an initial structure via a single-step atomic displacement along one (or several) low-frequency modes until a preset root-mean-square displacement (RMSD), typically 2.0–3.5 Å, between the two structures is attained. However, local dynamics, representative of a single near-native configuration, is generally inadequate for describing large-scale conformational rearrangements. In such processes the low frequency, highly collective protein normal modes (NMs) may well undergo dramatic changes in character, precisely features that cannot be captured in analyzing local dynamics. To account for such changes and establish gating pathways and transition-state structures, requires following or tracking the low-frequency NMs using an appropriate procedure [17,18].

All NMA approaches are vacuum simulations that ignore the influence of the surroundings. The underlying hypothesis, well established by long experience, is that large-scale conformational rearrangements are governed by the shape and backbone connectivity of the biomolecule itself, and the intrinsic directions of the cooperative displacements are effectively encoded in the native fold [19,20]. Placing a biomolecule in a realistic water/lipid environment results in overdamping the intrinsically allowed cooperative displacements encoded in the protein architecture [21]. Structural motion becomes slow and diffusive, not vibrational as in vacuum, meaning that the NM eigenvalues have no physical significance in terms of both the timescales and the amplitudes of harmonic oscillations as derived from eigenvalues. However, the NM eigenvectors are physically meaningful both in vacuum and in biophysically relevant milieus indicating the tendency of the protein structure to undergo a conformational change in a particular direction upon internal or external perturbations [20,21]. A biomolecular skeleton, alpha carbons connected by springs, placed in arbitrary surroundings is a purely harmonic system that follows a harmonic trajectory in the space of collective NM coordinates. However, this harmonic trajectory is altered by anharmonic contributions due to the presence of the side chains in a real protein and their diffusive, overdamped motion in a solvent [21]. Small conformational changes of the side chains and the surrounding's frictional effects are actually imposed on the large-scale motions of the backbone. Thus, the net effect of environmental influences on the structural dynamics of proteins evolving along gating pathways is to enforce an effectively harmonic trajectory [20,21]. The surroundings also may be significant if they can perturb the protein structure in ways that affect either shape or backbone connectivity.

Here we review our all-atom NMA results on gating initiation in five proteins (gA [22], KcsA [23], ClC-ec1 [24,25], LacY [26] and $LeuT_{Aa}$ [27]) and contrast these studies with analyses of gA and KcsA using our new methods, all-atom Monte Carlo Normal Mode Following (MC-NMF) [17] and its simplification, RTB MC-NMF [18], based on a rotation-translation of blocks (RTB) approximation [28]. Normal coordinates provide the collective degrees of freedom. Perturbing these proteins along the low-frequency NMs yields the largest collective structural changes at the smallest energetic cost. We show that cylindrically-shaped gA, KcsA, LacY and $LeuT_{Aa}$ biomolecules exhibit deformational modes reminiscent of global twisting, transverse and longitudinal motions in a homogeneous elastic rod. ClC-ec1's gross shape is totally different. Viewed perpendicular to the membrane plane it is rhomboid [29], but from within the membrane it looks somewhat like a butterfly. Its global deformations are also different. The subunits swing relative to one another, leading to a symmetric splay; its cytosolic and periplasmic regions alternate in electrolyte accessibility. We confirm anew the established fact that protein shape governs the character of the low-frequency NMs [19]. What conventional NMA-based methods cannot do is establish possible gating pathways because they do not describe changes in the collective coordinates during gating deformation. Our new methods are designed for just this purpose, and were applied to elucidate the large-scale conformational changes that take place in gA [17] and KcsA [18] along their gating pathways. In MC-NMF along their transition pathways, the continuous change of protein shape dramatically alters the global character of the low-frequency NMs. We discuss the effects of atomic level structure, hydrogen bonding and charged residues on large-scale conformational changes associated with gating.

2. Computational methods

2.1. Energy minimization and NMA

Minimization and harmonic analysis [7] are integral to our strategy for conformational searching of the relevant crystallographic structures. We treat these, incorporating explicit hydrogens, in full atomic detail. Structurally significant waters, ions and substrate molecules are retained, and the all-hydrogen CHARMM22 topology and parameter set [30] describes molecular systems. To remove atomic overlaps and relax the protein, we minimize using steepest descent with a random step length [7], which usually takes 500–2000 steps. The initially assembled molecular system is subject to a number of separate minimizations in Cartesian coordinates, each generating a different final configuration reflecting the random step length used in steepest descent [7]. All minimized structures conserve the native protein's fold, but each exhibits different side chain conformations. The lowest energy structure is selected and further minimized using a new nonlinear conjugate gradient method with guaranteed descent [31], one which is globally convergent. This approach is required to locate a geometry with unprecedentedly low strain energy ($<5\times10^{-10}$ kcal mol^{-1} Å^{-1}) for a large system (14,809 atoms in ClC-ec1). Other minimization methods such as standard Conjugate Gradient, Quasi-Newton, TNPACK and L-BFGS-B [7] do not converge. In order to carry out NMA on large proteins, the maximum derivative must be less than 10^{-8} kcal mol^{-1} Å^{-1} because low-frequency eigenvectors crucially reflect the quality of the minimized structure [7]. Properly minimized, the first six NMs, corresponding to translations and rotations of the whole molecule, must exhibit vibrational frequencies of zero. Imperfectly minimized, first-order terms in the Taylor expansion of the potential energy couple global molecular rotation with internal motions; these perturb the internal eigenvalues and eigenvectors, leading to apparent non-zero eigenvalues for the first six NMs. For maximum derivatives $>10^{-5}$ kcal mol^{-1} Å^{-1}, imaginary vibrational frequencies arise, indicating the structure is not properly minimized. Only in the fashion outlined are physically viable minima generated, with six zero and $3N-6$ positive eigenvalues [7].

NMA [7,12] approximates the full molecular potential by a harmonic function around a minimum energy structure. We approximate the CHARMM potential energy [30] E_c as a harmonic function E_h of the atomic mass-weighted Cartesian coordinates $\mathbf{x}$ around a stable conformation $\mathbf{x_0}$ using a Taylor expansion

$$E_h(\mathbf{x}) \approx E_c(\mathbf{x_0}) + \mathbf{g}^T(\mathbf{x}-\mathbf{x_0}) + \frac{1}{2}(\mathbf{x}-\mathbf{x_0})^T\mathbf{H}(\mathbf{x}-\mathbf{x_0}) \quad (1)$$

where $\mathbf{g}$ is the mass-weighted gradient vector, $\mathbf{x}-\mathbf{x_0}$ is the displacement vector and $\mathbf{H}$ is the mass-weighted Hessian matrix. The superscript T denotes the transpose of vectors $\mathbf{g}$ and $\mathbf{x}-\mathbf{x_0}$. For the bond and non-bonded energy terms the first and second derivatives of the potential energy E_c with respect to the mass-weighted Cartesian coordinates are calculated analytically. For other energy terms (angle, dihedral, improper and Urey–Bradley terms) a

modification of Ridders' method of polynomial extrapolation [32], a fourth-order finite-difference differentiation, is used to numerically calculate first and second derivatives (Hessian matrix). NMs are found by standard diagonalization of the Hessian, a $3N \times 3N$ matrix of second derivatives of the potential energy E_c with respect to the mass-weighted Cartesian coordinates. Eigenvalues and the corresponding eigenvectors are calculated using the eigensolver DSTEVR from the LAPACK library [33]. To enhance performance, highly optimized "building block" BLAS routines [34] are used to carry out basic vector and matrix operations.

2.2. All-Atom Monte Carlo Normal Mode Following

MC-NMF [17,18] combines NMA [12] and the eigenvector-following technique [35,36] with the Metropolis MC method [37]. Eigenvector following [36] establishes gating pathways and identifies saddle points. As NMA is performed at non-stationary points on the transition pathway, global translational and rotational modes are removed using the Eckart conditions [38], which spatially fixes the center-of-mass and constrains infinitesimal rotations. Mode-following [36] is initiated by a short Newton–Raphson step $\mathbf{h}_{NR} = -\sum_{i=1}^{3N} \bar{g}_i \mathbf{V}_i/\lambda_i$, where $\bar{g}_i$ is the component of the gradient $\mathbf{g}$ along the eigenvector $\mathbf{V}_i$ and λ_i is the ith eigenvalue; in each MC step $\mathbf{h}_{NR}$ is small and variable. A positive eigenvalue $\lambda_i > 0$ leads to a decrease of harmonic energy, $\Delta E_h = -\frac{1}{2}\sum_{i=1}^{3N} \bar{g}_i^2/\lambda_i$, along the associated $\mathbf{V}_i$ eigendirection, and a negative eigenvalue $\lambda_i < 0$ leads to energy increase. Properly choosing the sign of λ_i, the transition states (saddle points) on the potential energy surface are found by systematically maximizing the energy along the Hessian's lowest-frequency eigenvector while simultaneously minimizing the energy along orthogonal eigendirections [36]. In this way local (or global) minima can also be established by energy minimization along all NMs. New mass-weighted coordinates $\mathbf{x}$ are sampled as $\mathbf{x} = \mathbf{x}_0 + \xi \cdot \mathbf{h}_{NR}$ with ξ randomly chosen between 0 and 1. Moves along the gating pathway associated with the step $\xi \cdot \mathbf{h}_{NR}$ are accepted with a probability of $\min[1, \exp(-\Delta E_c/kT)]$ [37], where ΔE_c is the energy change calculated using the CHARMM22 potential energy. The full energy change ΔE_c is used, not its harmonic approximation ΔE_h. Simulations are performed at a T of 300 K. The Metropolis criterion [37] controls allowable MC step lengths. Each MC step involves the collective motions of large parts of the protein and is characterized by concerted conformational changes. Sampling is in a normal coordinate reference frame. If a new configuration $\mathbf{x}$ is accepted, then we *replace* $\mathbf{x_0}$ by $\mathbf{x}$, *rebuild* the Hessian matrix, *recalculate* gradients, eigenvectors and eigenvalues and *continue* with eigenvector following. After each accepted step, the all-atom Hessian matrix is *recalculated* and the eigensystem *solved* anew, for large proteins computationally very expensive. No constraints, restraints, artificial internal or external mechanical forces are imposed on the structure while tracking the lowest-frequency NM. This accounts for much of the protein's intrinsic motion along the reaction pathway. In moving along the transition pathway, the eigenvalues change resulting in a smooth change of eigendirections. The new lowest-frequency NM, the one most similar to the previous one, i.e. which has the largest overlap with it, is selected as the degree of freedom to be maximized. As overall translational and rotational motions are removed using the Eckart conditions [38], this procedure switches between eigendirections, ensuring that the desired uphill eigenvector, and properly identifying the one exacting the lowest energetic cost. Along the gating pathway, the lowest-frequency eigenvector changes with each MC step. After many steps, the initial (starting) and current low-frequency eigenvector sets differ significantly. By continuing along the lowest-frequency eigendirection we can locate saddles, transition states where all first derivatives of the potential energy with respect to the coordinates are zero and one eigenvalue is negative (a first-order saddle point). All-atom MC-NMF navigates among an energy surface's structurally different "deep minima," passing over the saddle points. Its focus is on movement of substantial protein segments in contrast to MD simulation, which samples local side chain rearrangements. Large biomolecules are usually composed of relatively rigid domains connected by flexible hinges. Therefore, small displacements of these flexible domains along the lowest-frequency eigenvector during MC-NMF lead to large amplitude structural changes.

To summarize, all-atom NMA generates the full spectrum ($3N$) of eigenvalues and eigenvectors (NMs). All are used in the MC-NMF method. The NM corresponding to the lowest eigenvalue is energy-maximized while the other NMs are energy-minimized. After each MC step, a new Hessian is built and the eigensystem is solved anew with the slightly different protein conformation. The NM spectrum has changed slightly, and the lowest-frequency NMs also differ. The procedure is then repeated, with the lowest eigenvalue NM in the new spectrum being energy-maximized. Thus, MC-NMF automatically switches among the low-frequency NMs, with no limitation on the number involved. Any of the low-frequency NMs can become the lowest-frequency NM.

2.3. RTB Monte Carlo Normal Mode Following

The RTB method [28] uses the full CHARMM22 energy function [30], but the protein is divided into rigid blocks, each consisting of one or a few consecutive segments. Thus, no information is lost with respect to electrostatic and other interactions [28]. The all-atom Hessian is projected onto a space spanning the rotational and translational degrees of freedom of predefined protein blocks, thus effectively reducing the Hessian matrix (to a size $6n_b \times 6n_b$ with n_b a number of blocks) and the diagonalization time. For each residue, a peptide backbone is treated as one block and, depending on residue size, the side chain is broken into zero (glycine and proline) to three (arginine and lysine) blocks. Each water molecule is a separate block and ions are associated with nearby rigid blocks. The $6n_b$-length RTB NMs are then projected back on the all-atom space giving a limited number, $6n_b$, of full-length ($3N_a$) approximate all-atom NMs. When the true all-atom NMs are substituted by approximate all-atom ones derived from the RTB approach, we find the original MC-NMF strategy fails because there are too few approximate NMs leading to insufficient relaxation of the high frequency NM subspace. This is avoided by separating maximization along the lowest-frequency NM from minimization along the other NMs, steps executed simultaneously in the original all-atom MC-NMF [17]. For each accepted maximization step, there is repeated minimization along the other NMs until the simulational system is relaxed. Thus, a single MC move (step) along the lowest-frequency NM involves a maximization step and numerous minimization steps. This modified RTB MC-NMF is reminiscent of our kinetic Monte Carlo Reaction Path Following approach [39], where motion is unidirectionally constrained along a predefined reaction coordinate and many MC trials are used to relax other degrees of freedom in each step along the reaction pathway. RTB MC-NMF [18], before applying it to large protein systems, was extensively tested and shown to properly describe gating behavior in gA [17,40].

3. Results

3.1. Lowest-frequency NM of gramicidin A from all-atom NMA and gating mechanism

The high-resolution structure of gA (PDB entry 1JNO [41]) was minimized (Fig. 1a) and standard vacuum all-mode NMA [12]

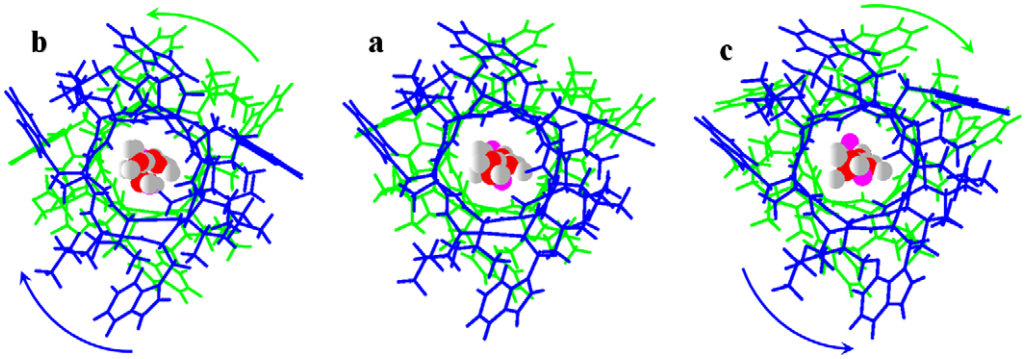

Fig. 1. Displacement of the atoms of the 1JNO system (a) along the eigenvector of the lowest-frequency mode (7th) in the two opposing directions termed "negative" (b) and "positive" (c). (a) The minimized 1JNO system, as viewed along the channel axis. gA monomers are colored blue and green. Ions and waters are shown in the pore. (b) The gA system displaced along the 7th eigenvector in the "negative" direction. Blue and green arrows show the direction of motion of each monomer. (c) The gA system displaced along the 7th eigenvector in the "positive" direction. This and the following figures were made by our MCICP code [46]. (For interpretation of the references to color in this figure legend, the reader is referred to the web version of this paper.). Reprinted, by permission, from Ref. 17.

applied to a system with the pore occupied by seven water molecules and two K^+, located at the binding sites. Minimization established a gA geometry with the least strain energy; all-atom NMA identified a lowest-frequency (7th) eigenvalue of $\sim$6.5 cm^{-1} (1 kcal/mol = 349.75 cm^{-1}) [17]. This minimized 1JNO system (Fig. 1a) was then perturbed along the 7th NM "negatively" (Fig. 1b) and "positively" (Fig. 1c), revealing relative monomer rotation in opposite directions around the pore axis. Displaced "negatively" (Fig. 1b), the blue monomer rotates clockwise, and the green one rotates anticlockwise. "Positive" rotations (Fig. 1c) reverse directionality. Near both channel mouths, the monomers are slightly distended, with larger atomic displacements than at the inter-monomer junction.

The lowest-frequency all-atom eigenvector was tracked in the "positive" direction via all-atom MC-NMF [17], which revealed the channel's gating mechanism: dissociation via coupled monomer counter-torsion and simultaneous lateral displacement. However, dissociation was not simply rigid-body monomer counter-torsion. It involves coupling inter-monomer hydrogen bond breaking, backbone realignment, and relative monomer tilt with complex side chain reorganization at the inter-monomer junction. Along the transition pathways we found multiple minima as well as transition-state conformers, with one negative eigenvalue characteristic of a saddle point. The stationary points (minima and saddle points) are geometries of lowest strain energy. As the side chains comprise a rich rotameric space, detailed transition pathways differ and gating proceeds with complex side chain reorganization and relative monomeric tilt. However, in all cases gA dissociation begins with relative opposed monomer rotation coupled with lateral displacement.

3.2. Lowest-frequency NM of KcsA from all-atom NMA and gating mechanism

The high-resolution KcsA structure (PDB entry 1K4C [42]) with three K^+ ions and 31 water molecules saturating the cavity and pore domains was used and all-atom NMA calculations performed [18]. Because KcsA gating requires cytosolic acidification [43], we studied WT KcsA and three variants with either or both sets of residues, E118 and E120, protonated. The 7th eigenvalue was slightly variant dependent, between 2.2 and 2.9 cm^{-1}; however, the associated eigenvectors were essentially identical. Perturbing the minimized WT structure along the 7th eigenvector is illustrated in Fig. 2, revealing a concerted, lever-like swinging of the TM2 and TM1 helices about pivot points near the C termini of the P helices (Fig. 2b and c) coupled with concerted rotation of the TM2 helical bundle around the channel axis [18]. The intracellular ends of the TM2 helices bend at A108 pivot points toward or away from the pore, respectively and the P-helices execute a swinging motion, but the selectivity filter's P-loops remain nearly rigid [44]. One might expect that protonating the E118 and E120 residues would facilitate outward-directed movement of the TM2 helices. However, this is not the case. Regardless of the glutamates' protonation states, the inner hydrophobic vestibule of KcsA remains closed in perturbing along the 7th eigenvector to an RMSD of 3.5 Å in a single-step move in either direction [18]. All-atom NMA could not identify the gating transition.

However, tracking via RTB MC-NMF showed very different behavior. With the residues E118 and E120 protonated (low interior pH), clockwise tracking along the lowest-frequency NM leads to complicated gating motions [18]. It involves concerted rotation and unwinding of the TM2 bundle with an outward bend of TM2 at A108, small twisting-untwisting rotations of the intracellular end of TM2 about a helical axis, and highly dynamic tilting adjustments and outward lateral motions of TM2 away from the channel axis leading to disruption of the TM2 bundle. The initial TM2 bend at A108 (common to all four protonation variants studied) propagates, for the fully protonated variant only, to a gating hinge near residues A98-G99. For the fully protonated variant alone, open-state KcsA exhibits a wide intracellular pore, with a radius $\sim$5–7 Å in the inner vestibule, located at the constriction near the T107 residues. The intracellular halves of the four TM1 and TM2 helices are loosely coupled and substantially separated. The central cavity is now an inseparable part of the cytosol.

3.3. Lowest-frequency NM of LacY symporter from all-atom NMA

A 3.5 Å resolution LacY structure (the C154G mutant, PDB entry 1PV6 [26]), a system of 6,625 protein atoms, one β-D-galactopyranosyl-l-thio-β-D-galactopyranoside (TDG) molecule (45 atoms) and 277 water molecules (831 atoms), a total of 7501 atoms formed the basis for NMA [45]. Due to low resolution, water molecules were not structurally resolved; they were introduced intracellularly using our MCICP code [46]. E325, located in a hydrophobic environment near the transporter center, and believed directly involved in proton translocation [26], was protonated. As the crystal structure was of the C154G mutant, trapped with an open intracellular pore, we reversed mutated, G154C, to obtain the native structure. For this protein five minimizations were effected, three for the E325p-G154C-LacY complex, denoted Nat-LacY, one for the unmutated LacY (denoted Cry-LacY) and one for this system with E325 protonated (E325p-Cry-LacY). All were loaded with TDG.

Fig. 2. Perturbation of the WT KcsA system along the 7th NM: (a–c) axial view from the intracellular side. (a) The minimized WT KcsA system; (b and c) displacement along seventh NM in the counterclockwise and clockwise directions, respectively. The three helices of each KcsA subunit are shown in backbone representation in the same color. The polypeptide loops are in gray. The location of A108 at the bundle crossing is marked in black. Pore water molecules and K^+ ions are explicitly shown. Arrows indicate the directions of rotation and displacement of the KcsA domains upon perturbation. (For interpretation of the references to color in this figure legend, the reader is referred to the web version of this paper.) Reprinted, by permission, from Ref. 18.

The RMSD for 417 C_α is 1.42 Å between the crystal and the five minimized LacY structures; the RMSD for all 6625 protein atoms is 1.75 Å; and, the RMSD for all 7501 atoms (including TDG and added waters) is 1.94 Å, all fairly small. Just as with gA and KcsA, small molecular changes have little effect on the lowest-frequency (7th) eigenvalue. It is nearly the same in all five systems: between 3.3 and 3.6 cm^{-1}. Similarly, 7th NM eigendirections are nearly identical in all five cases, with overlaps are ~1. Protonating E325 and/or mutating G154 had no significant effect on the 7th eigenvalue or eigenvector.

Perturbing Nat-LacY along the 7th all-atom NM initiates global counter-torsions of the cytoplasmic and periplasmic halves around the pore axis (curved arrows in Fig. 3 showing stills of video available online in Supplementary Data) [45]. The Cry-LacY and E325p-Cry-LacY systems displayed similar behavior; from here we focus on Nat-LacY. Its periplasmic half rotates clockwise and the cytoplasmic half anticlockwise, and vice versa. Coupled counter-torsion of the cytosolic and periplasmic halves of the TM helices is highly concerted and cooperative. The stationary plane relative to which rotation occurs passes through its center and is parallel to the membrane. As the cytoplasmic pore is open, the intracellular halves of the TM helices are loosely coupled as compared to the extracellular ones. However, rotation of the intracellular halves is also cooperative and concerted. The long polypeptide loop, located on the pore perimeter and connecting inter-domain TM6 and TM7, rotates (donut mark in Fig. 3). On the side opposite the pore, the N-terminus (connected to TM1) and the C-terminus (small helix connected to TM12) rotate around the pore axis. In perturbing to an RMSD of 3.5 Å along the 7th NM in either direction, the extracellular pore remains closed while there is noticeable, but still relatively insignificant (~1.0 Å), opening of the intracellular mouth. All-atom MC-NMF of the 7th NM, required to elucidate the proposed alternating access gating mechanism [26,47], convert between inward- and outward-facing LacY conformations, and establish dynamical differences between the three LacY variants analyzed, has yet to be carried out.

3.4. Lowest-frequency NM of $LeuT_{Aa}$ symporter from all-atom NMA

A high-resolution (1.65 Å) crystal structure of $LeuT_{Aa}$ (PDB entry 2A65 [27]), a molecular system of 8204 protein atoms, 210 water molecules, one leucine (Leu) molecule (22 atoms), two sodium ions and one chloride, totaling 8859 atoms was analyzed using NMA [48]. E419 was protonated; in the crystal structure its side chain is near the E62 residue (~2.6 Å). The bound Leu was treated as a zwitterion. Three independent minimizations were performed on the Leu–$LeuT_{Aa}$ system. Another minimization was performed on the Leu-free molecular system (Water–$LeuT_{Aa}$), replacing it by seven waters, totaling 8858 atoms. The RMSD between crystal and minimized $LeuT_{Aa}$ structures is 1.06 Å for 512 C_α; 1.33 Å for all 8204 protein atoms; and 1.49 Å for the full 8859 atom system (including waters). The 7th eigenvalue was nearly equal in all four systems, between 3.57 and 3.74 cm^{-1}. Replacing bound Leu by waters has no effect on the lowest-frequency eigendirections.

Perturbation of Leu–$LeuT_{Aa}$ along the 7th NM demonstrates highly concerted and cooperative counter-torsions of the

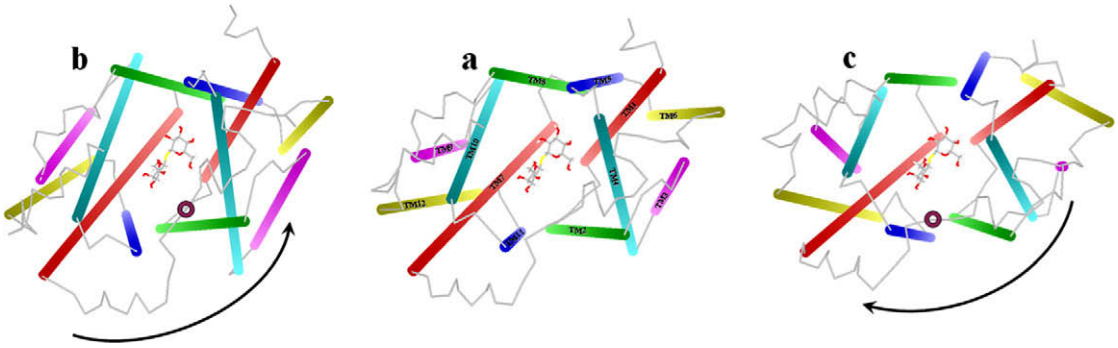

Fig. 3. Stills of video showing perturbation of the Nat–LacY system along the 7th NM. For clarity, added waters are not displayed. The lactose homolog, TDG, is sited at the sugar-binding site, the protein center. TM helices are shown as cylinders, with extra- and intracellular ends visualized in light and dark colors, respectively. Arrows indicate the directions of counter-torsions. View from the intracellular side: (a) the minimized system; (b and c) displacement along the 7th all-atom NMs in the "positive" and "negative" directions. Full video is available online in Supplementary Data. (For interpretation of the references to color in this figure legend, the reader is referred to the web version of this paper.)

intracellular and extracellular domains around the pore axis (curved arrows in Fig. 4 showing stills of video available online in Supplementary Data) [48]. Water–LeuT$_{Aa}$ displayed the same behavior. Extracellularly, overall rotation of the peripheral helices reconfigures the inner helices (TM1, TM6, TM3, TM8 and TM10). The V-shaped TM1 and TM6 helices alternately straighten (close) and bend (open) at their midpoint breaks (straight arrows in Fig. 4a). Similarly, near their midpoints TM8 and TM3 also alternately bend (open) and straighten (close). On the other side, large-scale movement of TM1 and TM6 is constrained by TM2 and TM7. Straightening TM1, TM6, TM3 and TM8 occludes the extracellular mouth, and bending expands it. Loops and small helices on the extracellular side undergo large-scale rotational motion. The intracellular domain of Leu–LeuT$_{Aa}$ rotates concertedly around the pore axis as nearly a rigid unit. The radial location of the intracellular ends of TM1a, TM6b, TM3 and TM8 relative to the pore is not affected. All-atom MC-NMF of the 7th NM, required to reveal the nature and detailed dynamics of the gating transition and to establish details of Leu involvement, has yet to be carried out.

3.5. Lowest-frequency NM of ClC-ec1 exchanger from all-atom NMA

Here we use the high-resolution (2.5 Å) X-ray structure of an *E. coli* ClC-ec1 antiporter (PDB entry 1OTS [25]) with four Cl^- at binding sites in the pores and 427 crystallographic waters as the basis for NMA [49]. Protein hydrogens were added via our MCICP code [46], yielding 13,524 protein atoms, and 14,809 overall. After energy minimization the C_α RMSD between crystal and minimized structures is 1.69 Å and the RMSD for all 14,809 atoms is 2.1 Å.

Perturbing the ClC-ec1 antiporter along the 7th all-atom NM in either direction (Fig. 5) leads to "butterfly-like" relative subunit swinging, perpendicular to a membrane plane [49]. The swivel axis lies in a membrane plane at the subunit interface near the protein's center. Black arrows indicate domain displacement directions upon perturbation. The intracellular part of the subunit interface (highlighted by the dotted red line within the blue oval of Fig. 5) is the region most affected. The two halves of the protein separate (Fig. 2b) and then approach closely (Fig. 2c). The intracellular ends of the H and I helices and their connecting polypeptide loops separate and approach (double-headed cyan arrow at the far end of Fig. 5's cytoplasmic region). The R and A helices undergo large scale swaying, thus increasing and decreasing the distance between their cytoplasmic ends. As the subunits separate, the intracellular pore tilt with respect to the membrane plane changes substantially. Thus the pore region between the two Cl^- ions constricts when perturbed "negatively" (Fig. 2c) and expands when perturbed "positively" (Fig. 2b). These regions, between the central and inner Cl^- ions, are highlighted by dotted red lines embedded in small blue triangles. In contrast, the extracellular regions and the main part of the subunit interface are much less affected, although there are some changes. The extracellular regions (dotted red lines embedded in large blue triangles in Fig. 5) structurally affected by the slow swinging subunit motion are localized near the extracellular Cl^- pathway. When perturbed "positively" (Fig. 2b), these domains compress (note rearrangements of the extracellular parts of peripheral helices at triangle marks relative to the helices I), possibly shutting the extracellular pores. When perturbed "negatively" (Fig. 2c), the extracellular regions near the conduction pathways relax, possibly opening the extracellular pores. Thus, the oval and triangles highlight the regions mainly contributing to the 7th NM. Overall, the protein alternately splays in and out.

While all-atom MC-NMF, needed to provide structural and molecular insight into how swinging the ClC subunits affects the chloride permeation pathways, has not yet been performed, NMA suggests a mechanism for Cl^-/H^+ exchange involving a conformational cycle of alternating exposure of Cl^- and H^+ binding sites of both ClC pores to the two sides of the membrane [50]. The intracellular and extracellular permeation pathways alternately close and open, in concert with the subunits' swinging motion. When outward facing, both extracellular pores are open and can bind Cl^- ions and both intracellular pores are closed with the proton sensitive E203 residues buried deeply in the protein interior. When inward facing, both extracellular pores are closed and both intracellular pores are opened for release of Cl^-; the E203 residues face the cytoplasm and are proton accessible.

4. Discussion

We carried out energy minimization and NMA studies of some quite different proteins [22–27]. NMs provide important information about the dynamics of the protein molecule [12]. NMA expresses the protein dynamics in terms of collective variables, the NM coordinates, which describe inherent collective displacements of protein atoms [7] and provide a suitable coordinate reference frame. NM treatments are designed to identify and characterize the slowest motions of macromolecular systems [51]. These slow modes are characteristic of a particular protein and related to its function [20,21]. Thus, the large number of degrees of freedom (~45,000 NMs for ClC-ec1) is reduced to an

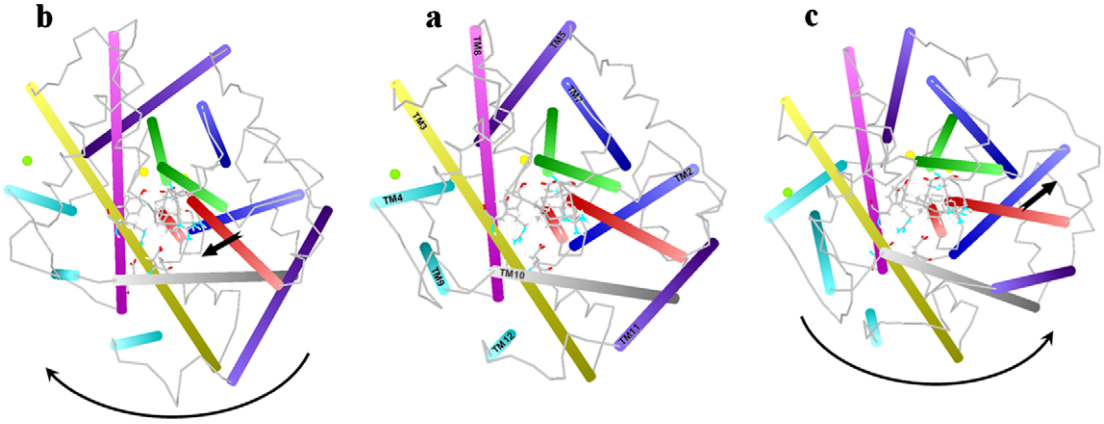

Fig. 4. Stills of video showing perturbation of the Leu–LeuT$_{Aa}$ system along the 7th NM. For clarity, crystallographic waters are not shown. Leu is shown at its binding site in the center of LeuT$_{Aa}$. TM helices are represented as cylinders, with extracellular and intracellular ends shown in light and dark colors, respectively. View from the extracellular side in a cylinder representation: (a) the minimized Leu–LeuT$_{Aa}$ system; (b and c) displacement along the 7th all-atom NM in the "negative" and "positive" directions. Full video is available online in Supplementary Data. (For interpretation of the references to color in this figure legend, the reader is referred to the web version of this paper.)

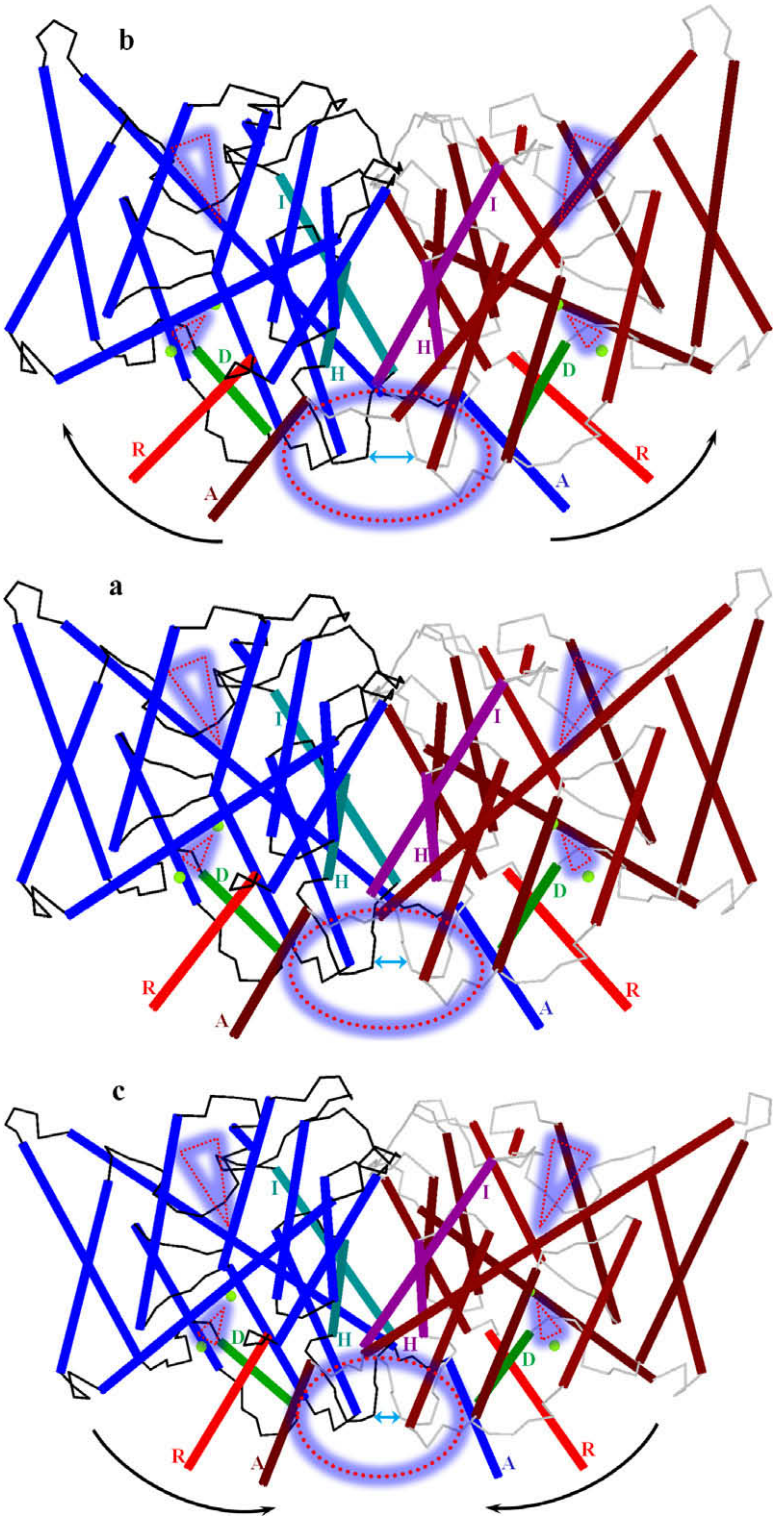

Fig. 5. Perturbation of the ClC-ec1 system along the lowest-frequency 7th NM. View from within a membrane plane with helices in cylinder representation. (a) The minimized system; (b) and (c), "positive" and "negative" displacement along the 7th all-atom NM. Helices H and I at the subunit interface are shown in dark magenta (subunit A) and dark cyan (subunit B). Helices R and D are shown for both subunits in red and green, respectively. The remaining subunit A helices are colored brown, and the subunit B ones are blue. Helices A near helices R of the other subunit are labeled. Polypeptide loops of subunits A and B are colored in gray and black, respectively. For clarity, crystallographic waters are suppressed. Four Cl^- ions (green spheres) are shown at the pores' central and interior binding sites. The pore lining residues S107, Y445, E148 and R147 are displayed. The E148 side chain blocks the periplasmic pore and side chains of S107 and Y445 constrict the cytoplasmic pore. The oval and triangles highlight the protein regions mostly affected in perturbation. (For interpretation of the references to color in this figure legend, the reader is referred to the web version of this paper.). Reprinted, by permission, from Ref. 50.

"essential space", where only a few low-frequency NMs matter. A set of these global or collective coordinates, retaining all atomic-level details, captures overall large-scale conformational changes of a biomolecule. The atomic coordinates, forming a set of local coordinates, are used to derive global coordinates. Thus, all-atom NMA introduces no reduction in the atomic complexity of a molecular

system. All-atom local coordinates are mapped to all-atom NM coordinates. A few of the low-frequency global NMs describe large-scale gating transitions in proteins, while high-frequency NMs describe local motions.

Collective coordinates describe overall fluctuations such as global counter-torsion of the intracellular and extracellular halves of the cylindrical gA, KcsA, LacY and $LeuT_{Aa}$ systems and global swinging of the subunits in "butterfly-like" ClC-ec1. The motions we discovered agree with much previous and subsequent work. Our predictions with respect to gA gating confirmed the experimental results of Harms et al. [52] in that (1) multiple open and closed states result from fluctuations at the inter-monomer junction, not from pore blockage by side chains occluding the mouth; (2) considerable variation in channel conductance involves no significant change in inter-monomer separation; (3) conformational fluctuations (flickers) in the open states result from fluctuations at the inter-monomer junction; (4) dynamics and kinetics of the gramicidin dimer are inhomogeneous and spatially confined due to gramicidin's helical structure making specific rotational and spatial demands on the relative monomer arrangement along the most favorable dissociation path. An independent theoretical study reporting NMA results on a native gA channel [53] found that the lowest-frequency NM ($\sim$6.8 cm^{-1}) is relative opposed monomer rotation (twisting) and simultaneous lateral displacement (bending) of gA, thus confirming our predictions regarding the onset of gating [17]. NMA of KcsA's intrinsic structural flexibility [54] revealed that each TM2 helix pivots on the intrasubunit hinge, located about 1/3 of the helix's length from the extracellular side, and that the TM2 helical bundle rotates concertedly around the channel axis at the intracellular side, observations agreeing completely with our KcsA analysis [18]. Recent work [55], with a gold nanocrystal attached to the cytoplasmic KcsA domain, unambiguously showed that upon cytoplasmic acidification the channel opens and the transmembrane helices rotate clockwise (viewed from the cytoplasmic side). Rotational motions around the channel's longitudinal axis predominated and far exceeded the radial expansion of the inner helices. From single-channel recordings of singly and doubly mutated KcsA [56], the two sets of cytoplasmic glutamates, E118 and E120, were identified as major influences on KcsA-gating, confirming our prediction [18] as to how charged residues near the C termini of TM2 affect gating. Recent structural comparisons of the LeuT-Leu ("outward-facing occluded") [27] and LeuT-Trp ("outward-facing open") [57] complexes demonstrate that there is an outward rotation of a protein group composed of TM1b, TM2 and TM6a about an axis oriented nearly parallel to the membrane and located near the unwound regions of TM1 and TM6, motions widening the extracellular mouth of $LeuT_{Aa}$. These results [57] agree with our earlier NMA observations on how the V-shaped TM1 and TM6 helices alternately straighten (close) and bend (open) at their midpoint breaks [48]. Experiments based on fluorescence resonance energy transfer showed that the C-termini of the ClC subunits undergo large relative movement [58]. Closure of both pores was accompanied by physically separating the two C-termini. Opening was accompanied by motion decreasing the C-termini separation. These experimental observations agree with our NMA prediction of large scale swaying of the R and A helices [49,50], an effect that increases and decreases the distance between their cytoplasmic ends.

The gA, KcsA, LacY and $LeuT_{Aa}$ proteins are cylindrically-shaped biomolecules. They can be considered as elastic rods of finite length, except for KcsA, which more closely resembles an inverted teepee [23,42]. Continuum mechanics indicates that typical deformational modes of a homogeneous elastic rod are twisting (torsion), transverse (bending) and longitudinal (stretching) NMs [59,60], motions characteristic of cylindrical geometries. For gA, LacY and $LeuT_{Aa}$, the concerted and cooperative counter-torsions of the intra- and extracellular halves are highly symmetric relative to the mid-membrane plane. For "conical" KcsA [42], this plane is located close to the C-termini of P-helices, $\sim$1/3 of the TM2 helix's length from the extracellular side. However, as the intracellular TM2 helical bundle rotates clockwise, the extracellular ends of TM2 rotate anticlockwise and vice versa. The amplitude of TM2's extracellular ends is significantly smaller. Nevertheless, KcsA exhibits low-frequency NMs characteristic of cylindrical proteins. But there are important protein specific differences. Our all-atom NMA data shows that the gA pore [17] and the KcsA selectivity filter [18,44] are not affected. The counter-torsions of LacY and $LeuT_{Aa}$ [45,48] affect the inner helices and the pore size quite differently. The transport cycle of LacY can involve a "rocker-switch" motion of the N- and C-terminal domains rotating about the sugar-binding site [61,62]. The transport mechanism of $LeuT_{Aa}$ can involve an "occlusion-switch" motion [57] where the substrate moves to the central binding site promoting blockage of the extracellular "open-to-out" vestibule and transforming the protein to the "open-to-in" state. The midpoint breaks of TM1 and TM6 provide a hinge around which conformational change can alternate [57]. Our all-atom NMA data [48] strongly argue that the V-shaped TM1 and TM6 pincers of $LeuT_{Aa}$ alternately straighten and bend at their midpoint breaks. Combining the three elastic rod collective motions can lead to other global motions. Consequently, elastic rod dynamics dominates at low frequencies, and it may be a general property of cylindrical biomolecules. However, the behavior of the other low-frequency NMs in these "cylindrical" proteins indicates that torsional and bending NMs contribute far more to the large-scale collective motions than pure stretching NMs. A possible explanation is that stretching NMs are substantially higher frequency because the effective force constants for stretching TM helices are relatively large due to the influence of hydrogen bonds.

ClC-ec1 is not a cylindrical protein [24,25]. Viewed perpendicular to the membrane this dimeric system is rhomboid, with major and minor diagonals of 100 and 55 Å, respectively [29]. Thus, one can expect a very different low-frequency NMs spectrum. Here, we found that the lowest-frequency NM describes a slow swinging motion of the ClC subunits relative to each other, perpendicular to a membrane plane [49,50], leading to inward and outward splay. This appears to be a general feature of ClC systems. ElNémo RTB NMA [63], which focuses on the influence of biomolecular shape and backbone connectivity, of a range of ClC mutant structures (PDB entries 2R9H (a straight-jacketed ClC-ec1), 1OTT (E148A), 1OTU (E148Q), 3DET (E148A/Y445A), 2HTL (Y445F), 2HT3 (Y445L), 2HLF (Y445E) and 2HT2 (Y445H)) all exhibited similar swinging subunit motions. Recent work has stressed that overall biomolecular shape dominates the behavior of low-frequency protein NMs [19]. This quantitative study shows that for large and densely packed proteins, low-frequency NMs are not sensitive to the local structure. Rather, they are highly anisotropic, and the allowed motions of biomolecules are shape-dictated [19].

Thus low-frequency NMs are determined by the global character of the structure-encoded collective deformations. They are dictated by overall protein shape, not local atomic details. This implies that a much simplified description, replacing the atomic force field by Hooke's law springs only linking each residue's C_α and treating these as point objects with three degrees of freedom (coarse-grained elastic NMA (eNMA)) [64,65], provides a reliable description. The justification for the RTB approximation [28] is that the low frequency RTB and all-atom NMA NMs are much alike. The inner products of the lowest-frequency (7th) RTB and all-atom NM eigenvectors are very similar. There are noticeable deviations in the 8th and 9th NMs, which become crucially different for higher-frequency NMs. Thus, the RTB and eNMA approaches provide a reliable way to identify the 7th NM, are useful for the 8th and 9th, and become invalid for higher-frequency NMs. All-atom and

coarse-grained NMA is only well suited for studying dynamics in a single potential well [13]. However, the conformational changes associated with a few low-frequency NMs, based on one particular minimized conformation of the system, are only indicative of inherent molecular flexibility. They provide no insight into the nature of a gating transition since this involves surmounting an activation energy barrier between at least two distinct conformations (potential wells), in other words coupling states with (most probably) totally different NM structures. Our all-atom NMA of the four "cylindrical" systems underscores this observation. It showed clearly that one-step displacements to a predefined RMSD along the low-frequency NMs are inadequate for elucidating the gating mechanism.

Identifying stationary points (saddles) connecting energy minima on multidimensional potential energy surfaces are very challenging for large systems. The all-atom and RTB MC-NMF methods [17,18] differ dramatically from standard NMA [7,12,13], which only explores protein dynamics about one near-native conformation. Tracking the lowest-frequency eigendirection, using these new techniques, permits identification of saddle points corresponding to transition-state structures. The NMA implemented in MC-NMF is performed at *non-stationary* points corresponding to distinct protein conformations along the transition pathway. As the conformations are distinct, NM structure also changes along the transition pathway. For "cylindrical" biomolecules, the lowest-frequency NM changes from a global counter-torsion to combined torsion-bending deformations, sometimes involving rotation of individual residues [17,18]. More importantly, biomolecular shape changes during MC-NMF along the gating pathway. The nature, global character and directionality of the 7th NM are automatically updated at each step of MC-NMF. In this approach, atomic-level details, including hydrogen bonding, are taken into account. We found that gating involves breaking quaternary networks (hydrogen bonds) in gA [17] and (salt bridges) in KcsA [18]. Hydrogen bonds at the gA inter-monomer junction break due to mechanistic, rotation–lateral monomer movement [17,40]. Opening the intracellular gate of KcsA requires salt bridge breaking triggered by cytoplasmic acidification of a network of ionized residues [18]. These examples clearly demonstrate the contribution of hydrogen-bonding and charged side chains (atomic structure details and electrostatics) to the gating process.

We are developing an approach accounting for all protein degrees of freedom, which is crucial for correctly describing the conformational change mechanism. No approximation (simplified potential functions, united C_α pseudo-atoms, rigid protein groups, etc.) other than the harmonic one is used in all-atom MC-NMF [17,18]. gA gating was studied with both all-atom and RTB MC-NMF [17], providing some useful insights. In RTB MC-NMF some fine details (inter-monomer hydrogen bond breaking, backbone realignment, relative monomer tilt, and especially side chain reorganization) of gA differed from results of all-atom MC-NMF. The rotameric reorganization (torsional motion) of side chains at the inter-monomer junction was affected. All-atom MC-NMF clearly shows that side chain rotation and reorganization precedes backbone motion. Along the gating pathway there are points where the lowest-frequency NM depicts local rotation (torsion) of a single side chain about a bond near the inter-monomer junction, a collective mode quite different from the initial global counter rotation of the two gA monomers. These motions were suppressed in RTB MC-NMF of gA, presumably due to rigid protein side chains. Furthermore, in RTB MC-NMF simulations, gA dissociation always proceeds directly without formation of transition-state conformers. In RTB MC-NMF of KcsA gating [18] no saddle points were detected. Preliminary RTB MC-NMF simulations of LacY gating [45] also failed to interconvert the open-in and open-out conformations about the TDG binding site, presumably reflecting the influence of the rigid protein blocks used. These observations clearly demonstrate the importance of using all-atom MC-NMF to study protein gating.

5. Summary

We first showed that normal coordinates provide a suitable coordinate reference frame for computational studies of protein gating transition. The cylindrically-shaped biomolecules, gA, KcsA, LacY and $LeuT_{Aa}$, demonstrate global torsion, bending and couplings characteristic of deformational modes of a homogeneous elastic rod. The global shape of biomolecules, not the local structure, establishes the permitted anisotropic motions in proteins [19]. All-atom and coarse-grained NMA are reliable ways to study the protein dynamics in a single potential well. However, these methods often do not yield a picture of the gating mechanism. All-atom and RTB MC-NMF methods, which explore transition states and structures corresponding to distinct protein conformations on the gating pathway are totally different from conventional NMA, which is limited to exploring conformational change in a single potential well (near-native conformation). Atomic structural details, hydrogen bonding and electrostatics all influence the nature of conformational changes on the gating pathway. Finally, approximations like coarse graining and rigid protein blocks can suppress significant structural rearrangements affecting protein gating transitions. Therefore, including and relaxing all system degrees of freedom are quite important in such studies.

Acknowledgements

This work was supported by a grant from the National Institutes of Health, GM-28643 and by Purdue University.

Appendix A. Supplementary data

Supplementary data associated with this article can be found, in the online version, at doi:10.1016/j.molstruc.2010.01.009.

References

[1] J. Drenth, Principles of Protein X-Ray Crystallography, Springer-Verlag, New York, 1999.
[2] S. Kundu, J.S. Melton, D.C. Sorensen, G.N. Phillips Jr., Biophys. J. 83 (2002) 723.
[3] H.M. Berman, J. Westbrook, Z. Feng, G. Gilliland, T.N. Bhat, H. Weissig, I.N. Shindyalov, P.E. Bourne, Nucleic Acids Res. 28 (2000) 235.
[4] T. Ha, Methods 25 (2001) 78.
[5] K. Wuthrich, NMR of Proteins and Nucleic Acids, Wiley-Interscience, New York, 1986.
[6] J.A. McCammon, S.C. Harvey, Dynamics of Proteins and Nucleic Acids, Cambridge University Press, 1987.
[7] A. Leach, Molecular Modelling: Principles and Applications, second ed, Prentice Hall, 2001.
[8] R.J. Mashl, E. Jakobsson, Biophys. J. 94 (2008) 4307.
[9] E.W.W. Ren, E. Vanden-Eijnden, Phys. Rev. B 66 (2002) 052301.
[10] A. Pan, D. Sezer, B. Roux, J. Phys. Chem. B 112 (2008) 3432.
[11] T. Baştuğ, P.C. Chen, S.M. Patra, S. Kuyucak, J. Chem. Phys. 128 (2008) 155104.
[12] M. Levitt, C. Sander, P.S. Stern, J. Mol. Biol. 181 (1985) 423.
[13] Qiang, I. Bahar, Normal Mode Analysis. Theory and Applications to Biological and Chemical Systems, Chapman & Hall/CRC, Boca Raton, FL, 2006.
[14] I. Bahar, A.J. Rader, Curr. Opin. Struct. Biol. 15 (2005) 586.
[15] M.A. Balsera, W. Wriggers, Y. Oono, K. Schulten, J. Phys. Chem. 100 (1996) 2567.
[16] A.L. Tournier, J.C. Smith, Phys. Rev. Lett. 91 (2003) 208106.
[17] G.V. Miloshevsky, P.C. Jordan, Structure 14 (2006) 1241.
[18] G.V. Miloshevsky, P.C. Jordan, Structure 15 (2007) 1654.
[19] M. Lu, J. Ma, Biophys. J. 89 (2005) 2395.
[20] J. Ma, Curr. Protein Pept. Sci. 5 (2004) 119.
[21] J. Ma, Structure 13 (2005) 373.
[22] O.S. Andersen, Annu. Rev. Physiol. 46 (1984) 531.
[23] D.A. Doyle, J.M. Cabral, R.A. Pfuetzner, A. Kuo, J.M. Gulbis, S.L. Cohen, B.T. Chait, R. MacKinnon, Science 280 (1998) 69.
[24] R. Dutzler, E.B. Campbell, M. Cadene, B.T. Chalt, R. MacKinnon, Nature 415 (2002) 287.

[25] R. Dutzler, E.B. Campbell, R. MacKinnon, Science 300 (2003) 108.
[26] J. Abramson, I. Smirnova, V. Kasho, G. Verner, H.R. Kaback, S. Iwata, Science 301 (2003) 610.
[27] A. Yamashita, S.K. Singh, T. Kawate, Y. Jin, E. Gouaux, Nature 437 (2005) 215.
[28] F. Tama, F.X. Gadea, O. Marques, Y.-H. Sanejouand, Proteins 41 (2000) 1.
[29] R. Dutzler, FEBS Lett. 564 (2004) 229.
[30] A.D. MacKerell Jr., D. Bashford, M. Bellott, R.L. Dunbrack Jr., J.D. Evanseck, M.J. Field, S. Fischer, J. Gao, H. Guo, S. Ha, D. Joseph-McCarthy, L. Kuchnir, K. Kuczera, F.T.K. Lau, C. Mattos, S. Michnick, T. Ngo, D.T. Nguyen, B. Prodhom, W.E. Reiher III, B. Roux, M. Schlenkrich, J.C. Smith, R. Stote, J. Straub, M. Watanabe, J. Wiorkiewicz-Kuczera, D. Yin, M. Karplus, J. Phys. Chem. B 102 (1998) 3586.
[31] W.W. Hager, H. Zhang, SIAM J. Optim. 16 (2005) 170.
[32] C.J.F. Ridders, Adv. Eng. Software 4 (1982) 75.
[33] E. Anderson, Z. Bai, C. Bischof, S. Blackford, J. Demmel, J. Dongarra, J. Du Croz, A. Greenbaum, S. Hammarling, A. McKenney, D. Sorensen, LAPACK Users' Guide, third ed., SIAM, Philadelphia, PA, 1999.
[34] J.J. Dongarra, J. Du Croz, S. Hammarling, I.S. Duff, ACM Trans. Math. Soft. 16 (1990) 1.
[35] J. Baker, J. Comput. Chem. 4 (1986) 385.
[36] J. Nichols, H. Taylor, P. Schmidt, J. Simons, J. Chem. Phys. 92 (1990) 340.
[37] N. Metropolis, A. Rosenbluth, M. Rosenbluth, A. Teller, E. Teller, J. Chem. Phys. 21 (1953) 1087.
[38] C. Eckart, Phys. Rev. 47 (1935) 552.
[39] G.V. Miloshevsky, P.C. Jordan, J. Chem. Phys. 122 (2005) 214901.
[40] G.V. Miloshevsky, P.C. Jordan, Biophys. J. 86 (2004) 92.
[41] R.R. Ketchem, K.C. Lee, S. Huo, T.A. Cross, J. Biomol. NMR 8 (1996) 1.
[42] Y. Zhou, J.H. Morais-Cabral, A. Kaufman, R. MacKinnon, Nature 414 (2001) 43.
[43] L. Heginbotham, M. LeMasurier, L. Kolmakova-Partensky, C. Miller, J. Gen. Physiol. 114 (1999) 551.
[44] G.V. Miloshevsky, P.C. Jordan, Biophys. J. 95 (2008) 3239.
[45] G.V. Miloshevsky, P.C. Jordan, Biophys. J. 94 (2008) 724–Pos.
[46] G.V. Miloshevsky, P.C. Jordan, Biophys. J. 86 (2004) 825.
[47] O. Jardetzky, Nature 211 (1966) 969.
[48] G.V. Miloshevsky, P.C. Jordan, Biophys. J. 94 (2008) 730–Pos.
[49] G.V. Miloshevsky, A. Hassanein, P.C. Jordan, Biophys. J. 96 (2009) 2426–Pos.
[50] G.V. Miloshevsky, A. Hassanein, P.C. Jordan, Biophys. J. 98 (2010), in press.
[51] M. Rueda, P. Chacón, M. Orozco, Structure 15 (2007) 565.
[52] G.S. Harms, G. Orr, M. Montal, B.D. Thrall, S.D. Colson, H.P. Lu, Biophys. J. 85 (2003) 1826.
[53] T. Mori, H. Kokubo, H. Shimizu, M. Iwamoto, S. Oiki, Y. Okamoto, J. Phys. Soc. Jpn 76 (2007) 094801.
[54] Y. Shen, Y. Kong, J. Ma, Proc. Natl. Acad. Sci. USA 99 (2002) 1949.
[55] H. Shimizu, M. Iwamoto, T. Konno, A. Nihei, Y.C. Sasaki, S. Oiki, Cell 132 (2008) 67.
[56] A.N. Thompson, D.J. Posson, P.V. Parsa, C.M. Nimigean, Proc. Natl. Acad. Sci. USA 105 (2008) 6900.
[57] S.K. Singh, C.L. Piscitelli, A. Yamashita, E. Gouaux, Science 322 (2008) 1655.
[58] E.A. Bykova, X.D. Zhang, T.-Y. Chen, J. Zheng, Nat. Struct. Biol. 13 (2006) 1115.
[59] L.D. Landau, E.M. Lifshitz, Mechanics-Course of Theoretical Physics, third ed., vol. 1, Butterworth, Washington, DC, 1982.
[60] B. Lautrup, Physics of Continuous Matter, Institute of Physics, University of Reading, Berkshire, 2005.
[61] L. Guan, O. Mirza, G. Verner, S. Iwata, H.R. Kaback, Proc. Natl. Acad. Sci. USA 104 (2007) 15294.
[62] Y.G. Zhou, L. Guan, J.A. Freites, H.R. Kaback, Proc. Natl. Acad. Sci. USA 105 (2008) 3774.
[63] K. Suhre, Y.-H. Sanejouand, Nucleic Acids Res. 32 (2004) W610.
[64] M.M. Tirion, Phys. Rev. Lett. 77 (1996) 1905.
[65] I. Bahar, A.R. Atilgan, B. Erman, Folding Des. 2 (1997) 173.